

Nonequilibrium electronic transport through a polymer chain: Role of solitons

Jia Wang, Yue Yang, Yao Yao, and Chang-Qin Wu*

Department of Physics and State Key Laboratory of Surface Physics, Fudan University, Shanghai 200433, China

(Dated: March 8, 2013)

Nonequilibrium electronic transport through a polymer chain is investigated by the scattering state operator method. The polymer chain is described by an electron-lattice coupling model and its two ends are connected with metal electrodes of different chemical potentials. The scattering states are shown to be a set of complete eigenstates of electrons in the system at nonequilibrium steady state. With the method, we show that the nonequilibrium Peierls transition (NEPT) does not survive the lattice relaxation and the soliton-antisoliton pair excitations. Furthermore the electronic transport through the chain is shown to be accomplished through the soliton-lattice energy band.

PACS numbers: 73.40.Sx, 72.10.-d, 71.20.Rv

I. INTRODUCTION

Molecular electronic devices are attracting great interests because of their tremendous advantages in applications. A lot of works are focused on electronic transport through a sandwich structure. For example, the measurement of conductance in a single molecule, such as a single conjugated polymer wire coupled with metallic leads, is recently developed to a more precise level than before using many different experimental methods.¹⁻⁶ To advance electronic devices at the single-molecule scale, we are in an increasing need for understanding the detail of charge transport through an individual molecule.

Theoretically, a nonadiabatic dynamical evolution method has been used in the studies for the polaron formation and motion in a polymer chain.⁷⁻⁹ In these studies, the metal electrodes are treated as finite chains due to the limitation of numerical computation and then it's not applicable to a long-time steady-state. To get a steady-state condition, the electrodes are better to be considered as (infinite) reservoirs. When the system is staying in a steady state with a constant particle/energy flow, i.e. a nonequilibrium steady state (NESS), the quantum statistical property becomes quite different from that in the equilibrium case. It is the special statistical property that plays an essential role in the formation of the flow and the behaviors of the polymer chain.

Non-equilibrium Green's function techniques are used widely in the mesoscopic transport problems.¹⁰ Using these methods, noninteracting problems could be solved exactly. For systems with many-body interactions, it involves summing a set of real time correlation functions for the linear, quadratic, cubic, etc, response to these interactions. Perturbation theory has succeeded in many problems before. Today, with great advances in experiments, there are more and more problems for which the nonperturbative methods are necessary and essential. A different approach called scattering state operator method, is focused on the construction of steady-state nonequilibrium ensemble.¹¹ In this method, nonequilibrium quantum statistical mechanics for steady state is written in a form similar to that in equilibrium case. Hershfield¹¹ has shown the existence of a statis-

tical operator Y which accounts for the nonequilibrium boundary condition as a part of an effective Hamiltonian. And he proposed that Y be constructed in terms of the scattering state operators. Once Y operator is constructed, the concepts in the equilibrium case and the equilibrium numerical techniques can be applied to nonequilibrium steady state only if H is replaced by $H_{\text{noneq}} = H - Y$. And the well-established equilibrium numerical techniques, such as exact diagonalization, the quantum Monte Carlo method, renormalization group, variational methods, etc, can bring great improvements if applied to nonequilibrium steady state.

Recently, Han *et al.* have done much based on the scattering state operator method.¹² They established the method by explicitly solving the electronic transport through a noninteracting single quantum dot (QD). Then the method is applied to a single QD with electron-phonon or electron-electron interactions and various transport phenomena are reproduced which have been studies before using other methods such as nonequilibrium Green's function techniques. This work is to generalize a single quantum dot to a quantum chain with some sites. We solve the transport through a fixed disordered chain without electron-phonon interactions explicitly, and then apply the method to a polymer chain that is described by the Su-Schrieffer-Heeger (SSH) model¹³ with electron-lattice interactions. The work provides a ground for the further generalization to the quantum chain with many-body interactions.

We consider the metal electrodes as large reservoirs and adopt the scattering state operator method to investigate the nonequilibrium electronic transport through a polymer chain coupled with the reservoirs. By the scattering operator method, we show that nonequilibrium Peierls transition (NEPT) does not survive the lattice relaxation and the soliton-antisoliton pair excitations, which is in contrary with the result of a previous work based on the continuum version of SSH model with the order parameter is assumed to be a constant.¹⁴ Furthermore, we show that a soliton lattice¹⁵ is formed in the NESS and the electronic transport is accomplished through the soliton-lattice energy band.

The arrangement of this article is as follows. In

the following section, we give our model for the metal/polymer/metal structure and describe the scattering state operator method. Numerical results are presented in Sec. III. The conclusions of this article are given in Sec. IV and details of calculations are given in the appendixes.

II. MODEL AND METHOD

A. Model Hamiltonian

We consider a sandwich structure which consists of a polymer chain and two metal electrodes coupled with the chain's two ends. The Hamiltonian of the whole system is composed of three terms as follows:

$$H = H_S + H_B + V, \quad (1)$$

where H_S is the Su-Schrieffer-Heeger (SSH) model, which describes the polymer chain of N -sites,

$$H_S = H_{\text{el}} + H_{\text{latt}} \quad (2)$$

with the electronic part as

$$H_{\text{el}} = - \sum_{n=1, \sigma}^{N-1} t_n \left(c_{n, \sigma}^\dagger c_{n+1, \sigma} + c_{n+1, \sigma}^\dagger c_{n, \sigma} \right), \quad (3)$$

where $t_n [\equiv t_0 - \alpha(u_{n+1} - u_n)]$ is the hopping integral between sites n and $n+1$ with t_0 being the one in an equidistance lattice, α describing the electron-lattice coupling between neighboring sites, and u_n the monomer displacement of site n from its equidistant position due to the electron-lattice interaction, and $c_{n, \sigma}^\dagger (c_{n, \sigma})$ is the creation (annihilation) operator for electron with spin σ at site n , and the lattice part of the chain as

$$H_{\text{latt}} = \frac{K}{2} \sum_{n=1}^{N-1} (u_{n+1} - u_n)^2 + \frac{M}{2} \sum_{n=1}^N \dot{u}_n^2, \quad (4)$$

where K is the elastic constant due to the σ bonds of the polymer chain and M the mass of a site that constitutes the chain. The metal electrodes are described by reservoirs of free electrons

$$H_B = \sum_{ak\sigma} \epsilon_{ak} d_{ak\sigma}^\dagger d_{ak\sigma}, \quad (5)$$

where $a (= L, R)$ indicates the left and the right metal reservoirs and $d_{ak\sigma}^\dagger (d_{ak\sigma})$ is the creation (annihilation) operator for electron with energy ϵ_{ak} and spin σ in the a electrode. The last term in the whole Hamiltonian is the coupling between the electrodes and the polymer chain, which gives as

$$V = \sum_{ak\sigma} g_{ak} \left(d_{ak\sigma}^\dagger c_{a\sigma} + c_{a\sigma}^\dagger d_{ak\sigma} \right), \quad (6)$$

where g_{ak} is the coupling between the a electrode and the site that is attached at the electrode, here, we fixed the site by $c_{L(R)\sigma} \equiv c_{1(N)\sigma}$, that is, the first ($n=1$) site of the chain is coupled with the left electrode while the last ($n=N$) site with the right electrode.

B. Scattering State Operators Method

The scattering state operator $\psi_{ak\sigma}^\dagger$ satisfies the Lippman-Schwinger equation as follows:

$$\psi_{ak\sigma}^\dagger = d_{ak\sigma}^\dagger + \frac{1}{\epsilon_{ak} - \mathcal{L}_0 + i\eta} [V, \psi_{ak\sigma}^\dagger], \quad (7)$$

where η is an infinitesimal convergence factor. The Liouville operator \mathcal{L}_0 is defined as $\mathcal{L}_0 A \equiv [H_0, A]$. The scattering state $|\psi_{ak\sigma}\rangle$ includes forward and backward scattering on the reservoirs and the molecule chain as well as the incoming reservoir state $|d_{ak\sigma}\rangle$. And the Lippman-Schwinger equation can be rewritten into the Heisenberg's equation of motion as follows:

$$[H, \psi_{ak\sigma}^\dagger] = \epsilon_{ak} \psi_{ak\sigma}^\dagger + i\eta (\psi_{ak\sigma}^\dagger - d_{ak\sigma}^\dagger). \quad (8)$$

First, we consider a fixed-lattice chain with a set of hopping integrals $\{t_n\}$. The scattering state operator $\psi_{ak\sigma}^\dagger$ can be expanded within the one-particle basis $\{d_{bk'\sigma}^\dagger, c_{n,\sigma}^\dagger\}$ as

$$\psi_{ak\sigma}^\dagger = d_{ak\sigma}^\dagger + \sum_{n=1}^N \gamma_n^{ak} c_{n,\sigma}^\dagger + \sum_{bk'} \gamma_{bk'}^{ak} d_{bk'\sigma}^\dagger. \quad (9)$$

By inserting Eq.(9) into Eq.(8), we obtain

$$\gamma_{bk'}^{ak} = \frac{g_{bk'}}{\epsilon_{ak} - \epsilon_{bk'} + i\eta} \gamma_b^{ak}, \quad (10)$$

(here, we have used $\gamma_L^{ak} \equiv \gamma_1^{ak}$ and $\gamma_R^{ak} \equiv \gamma_N^{ak}$.) and equations for $\{\gamma_n^{ak}\}$

$$\begin{aligned} (\epsilon_{ak} + i\Gamma_L) \gamma_1^{ak} + t_1 \gamma_2^{ak} &= g_{ak} \delta_{a,L}; \\ t_{n-1} \gamma_{n-1}^{ak} + \epsilon_{ak} \gamma_n^{ak} + t_n \gamma_{n+1}^{ak} &= 0 \quad (\text{for } n = 2, 3, \dots, N-1); \\ t_{N-1} \gamma_{N-1}^{ak} + (\epsilon_{ak} + i\Gamma_R) \gamma_N^{ak} &= g_{ak} \delta_{a,R}, \end{aligned} \quad (11)$$

where we have defined the density of states (DOS) of the reservoirs

$$\Gamma_a(\epsilon) = i \sum_k \frac{|g_{ak}|^2}{\epsilon - \epsilon_{ak} + i\eta}. \quad (12)$$

In the large bandwidth limit, the functions $\Gamma_a(\epsilon)$ are energy-independent constants. From the above equations, γ_n^{ak} can be written as

$$\gamma_n^{ak} = g_{ak} F_n^{(a)}(\epsilon_{ak}), \quad (13)$$

then we can obtain the functions $F_n^{(a)}(\epsilon)$, that are given in the appendix A.

As done by Han,¹² we can also show the completeness of the scattering state operators $\psi_{ak\sigma}^\dagger$ defined above under the assumption that there exist no isolated energy eigenstates in the NESS, that gives

$$\sum_{ak} \psi_{ak\sigma}^\dagger \psi_{ak\sigma} = \sum_{ak} d_{ak\sigma}^\dagger d_{ak\sigma} + \sum_{n=1}^N c_{n,\sigma}^\dagger c_{n,\sigma}, \quad (14)$$

which guarantees the original operators $\{d_{ak\sigma}^\dagger, c_{n,\sigma}^\dagger\}$ can be conversely represented by the scattering state operators $\{\psi_{ak\sigma}^\dagger\}$, which gives

$$d_{ak\sigma}^\dagger = \psi_{ak\sigma}^\dagger + \sum_{bk'} (\gamma_{ak'}^{bk'})^* \psi_{bk'\sigma}^\dagger, \quad c_{n,\sigma}^\dagger = \sum_{ak} (\gamma_n^{ak})^* \psi_{ak\sigma}^\dagger. \quad (15)$$

Furthermore, it can also be shown that the total Hamiltonian in Eq.(1) can be represented by the scattering state operators as follows:

$$H = \sum_{ak\sigma} \epsilon_{ak} \psi_{ak\sigma}^\dagger \psi_{ak\sigma}. \quad (16)$$

Then we have the effective Hamiltonian for the NESS¹¹

$$H_{\text{eff}} \equiv H - Y = \sum_{ak\sigma} (\epsilon_{ak} - \mu_a) \psi_{ak\sigma}^\dagger \psi_{ak\sigma}, \quad (17)$$

which leads immediately

$$\begin{aligned} \langle \psi_{ak\sigma}^\dagger \psi_{bk'\sigma'} \rangle &\equiv \frac{\text{Tr}\{e^{-\beta H_{\text{eff}}} \psi_{ak\sigma}^\dagger \psi_{bk'\sigma'}\}}{\text{Tr}\{e^{-\beta H_{\text{eff}}}\}} \\ &= f_a(\epsilon_{ak}) \delta_{a,b} \delta_{\sigma,\sigma'} \delta_{k,k'}, \end{aligned} \quad (18)$$

where $\langle \dots \rangle$ stands for the average with respect to the NESS, and $f_a(\epsilon) \equiv 1/(e^{(\epsilon - \mu_a)/kT} + 1)$ is the Fermi distribution function, μ_a being chemical potential of the a electrode.

C. Current at Nonequilibrium Steady State

Now we can calculate the current flow in the sandwich structure. The current from the left electrode to the polymer chain is given as usual,

$$I = \frac{ie}{\hbar} \sum_{k\sigma} g_{Lk} \left(\langle d_{Lk\sigma}^\dagger c_{1,\sigma} \rangle - \langle c_{1,\sigma}^\dagger d_{Lk\sigma} \rangle \right). \quad (19)$$

With respect to $\psi_{ak\sigma}^\dagger$, the current flow can be evaluated and finally represented as the Landauer-Büttiker form

$$I = \frac{2e}{h} \int d\epsilon T(\epsilon) [f_L(\epsilon) - f_R(\epsilon)], \quad (20)$$

where $T(\epsilon)$ is transmission rate, which can be determined by the coefficients $\{\gamma_n^{ak}\}$ and $\{\gamma_{bk'}^{ak}\}$, it gives

$$T(\epsilon) = 4\Gamma_L \Gamma_R |F_1^{(R)}(\epsilon)|^2. \quad (21)$$

With the same process, the current between neighboring sites in the polymer chain and that from the chain to the right electrode can be obtained. With the Eqs.(10-13), it is easily proved that all them are the same, which meets the requirement of a steady state (See Appendix B).

D. Lattice Relaxation at Nonequilibrium State

Now we consider the flexible lattice which we treat classically in this work. Since the mass of sites in the polymer chain is much heavier than that of electrons, the Born-Oppenheimer approximation is applicable. Then the force exerting on the polymer sites from the electron-lattice interaction could be obtained from the Hellmann-Feynman theorem. Furthermore, we consider the system to be at zero temperature, then the damping induced by exterior environment should eventually make the lattice at rest. At the steady state the force exerting on the lattice should be canceled out, which gives

$$y_n = (-1)^{n+1} \left(\frac{\lambda\pi}{2} \rho_{n,n+1} + \delta \right), \quad (22)$$

where we have defined the dimensionless staggered lattice order parameter $y_n = (-1)^n \alpha(u_{n+1} - u_n)/t_0$, the dimensionless electron-lattice coupling constant $\lambda = 2\alpha^2/(\pi K t_0)$, the bond-charge density $\rho_{n,n+1} = \sum_{\sigma} \langle c_{n,\sigma}^\dagger c_{n+1,\sigma} + \text{h.c.} \rangle$, with δ being a Lagrangian multiplier to guarantee the polymer chain length unchanged ($\sum_n (u_{n+1} - u_n) = 0$). By using Eq.(13), (15), and (18), we have

$$\rho_{n,n+1} = \sum_a \frac{4\Gamma_a}{\pi} \int d\epsilon \text{Re} \left[F_n^{(a)*}(\epsilon) F_{n+1}^{(a)}(\epsilon) \right] f_a(\epsilon). \quad (23)$$

III. NUMERICAL RESULTS

For the sake of simplicity, we consider a symmetric case in which the couplings with the electrodes are the same, *i.e.*, $\Gamma_L = \Gamma_R = \Gamma$, and the chemical potentials of the two electrodes are taken as $\mu_L = -\mu_R = V_b/2$ with V_b being the applied bias voltage. Furthermore, we take $t_0 (= 1)$ as the unit of energy and the dimensionless electron-lattice coupling constant $\lambda = 0.2$ in accord with that for *trans*-polyacetylene.

A. Lattice Configuration at Zero Bias Voltage

Before we present our results on steady current through a polymer chain and the role of solitons in it, the effects onto the polymer chain arising from the couplings with the reservoirs under equilibrium case ($V_b = 0$) are studied. As is well known, the lattice is dimerized due to the Peierls instability for an isolated polymer chain. The staggered lattice order parameter $y_n \approx 0.13$ except a few bonds near its two ends which are affected by the boundary condition. The zigzag of the order parameter is due to the finite-size effect under the restriction of chain-length unchanged. When the couplings to the reservoirs are turned on, the lattice configuration is affected by the reservoirs as shown in Fig. 1. It is clear that with weak couplings, such as $\Gamma = 0.26$ in Fig. 1(a), the lattice configuration should be very similar to that of an isolated

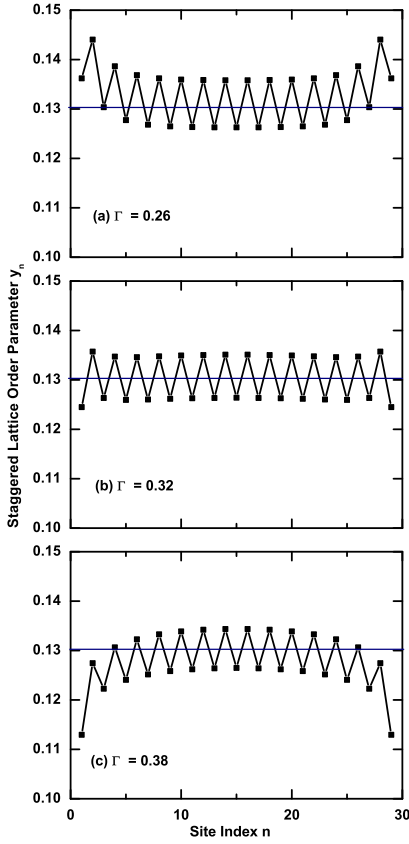


FIG. 1: The staggered lattice order parameter $\{y_n\}$ of a 30-site chain under different couplings with metal electrodes without applied bias voltage. The coupling constants are taken as $\Gamma = 0.26$ (a), 0.32 (b), and 0.38 (c). The straight line indicates the dimerization magnitude at thermodynamic limit.

chain, but a slight reduction of the order parameters near the ends, which makes the bond-length changes smaller than that for a free boundary condition. Once the coupling Γ is increased to an intermediate value $\Gamma = 0.32$ in Fig. 1(b), the bond-length changes at the chain ends become almost similar as that of the inside bonds. The boundary effect on the bond-length at the chain ends is canceled out by the couplings with the metal electrodes. When the couplings are enlarged more, such as $\Gamma = 0.38$, y_n for the bonds near the two ends are much less than 0.13 , which is opposite to that of an isolated chain with a free boundary condition (Fig. 1(c)). In the following, we take the intermediate coupling $\Gamma = 0.32$.

B. Lattice Configuration at Finite Bias Voltage

First, we see the lattice configuration at a finite bias voltage, which is shown in Fig. 2. It can be seen that the lattice has a little change under a small bias voltage, and then with increasing bias voltage, the lattice contains one soliton-antisoliton (SS) pair for $V_b = 0.56$ and two

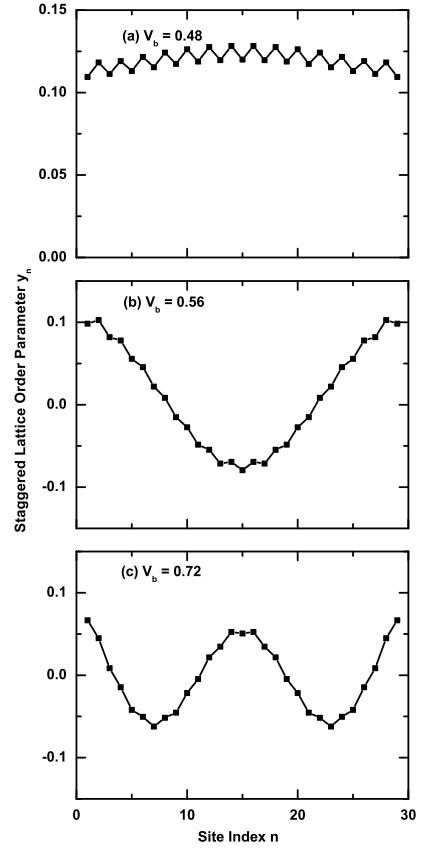


FIG. 2: The staggered lattice order parameter $\{y_n\}$ of a 30-site chain coupled with metal electrodes with a voltage bias $V_b = 0.48$ (a), 0.56 (b), and 0.72 (c). The coupling constant $\Gamma = 0.32$.

SS pairs for $V_b = 0.72$. It's expected the number of SS pairs will be increased one by one and a soliton lattice is formed at thermodynamic limit. To understand the formation of SS pairs in the polymer chain, we show the corresponding transmission rate $T(\epsilon)$ in Fig. 3. When V_b is below than 0.5 , electrons from the reservoirs can hardly flow to the polymer chain, due to the gap existing in the energy band of the polymer. $\{y_n\}$ shown in Fig. 2(a) is similar to that of an isolated polymer chain and $T(\epsilon)$ is shown in Fig. 3(a). When V_b is above a critical value, such as $V_b = 0.56$, the Fermi surface in the left reservoir reaches the $n = +1$ energy level of the polymer chain while the Fermi surface in the right is below $n = -1$ energy level (see Fig. 4). Since the whole system is on steady state, the $n = +1$ level is always occupied by electrons from the left reservoir and electrons on the $n = -1$ level flows to the right persistently. In all the polymer chain has no extra electrons since the bias voltage is added symmetrically, which corresponds to that an electron on $n = -1$ level is excited to the $n = +1$ level, as shown in Fig. 4(b). In order to minimize the total energy of the whole system, the polymer chain will be relaxed and a SS pair is formed (Fig. 4(c) and Fig. 2(b)). Transmission rate in the new $\{y_n\}$ is given in Fig. 3(b),

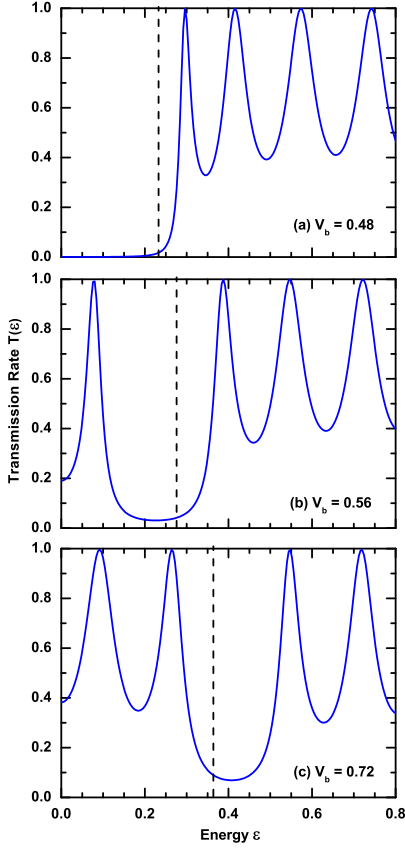


FIG. 3: The transmission rate $T(\epsilon)$ of a 30-site chain coupled with metal electrodes with a voltage bias $V_b = 0.48$ (a), 0.56 (b), and 0.72 (c). The coupling constant $\Gamma = 0.32$. The dashed lines indicate the Fermi levels of reservoirs.

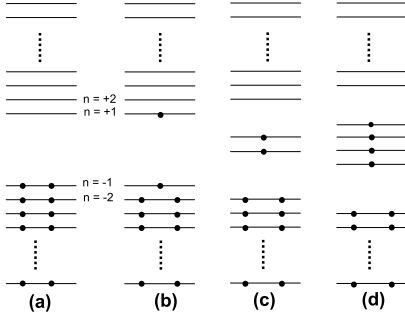


FIG. 4: Schematic energy-level diagram of a polymer chain for the formation of a soliton lattice. (a) A dimerized lattice with half-filled electronic band; (b) A dimerized lattice with one electronic excitation from a half-filled band; (c) One SS pair excited and (d) two SS pairs excited electronic band.

from which you can see one peak is moved down due to the SS pair formation for the energy levels of the solitons located inside the gap. It can be seen that the gap is moved up and matched the Fermi levels of reservoirs. Except the gap, other vales in the transmission rate shown in Fig. 3 are caused by the finite size of the chain and should disappear at thermodynamic limit. When V_b in-

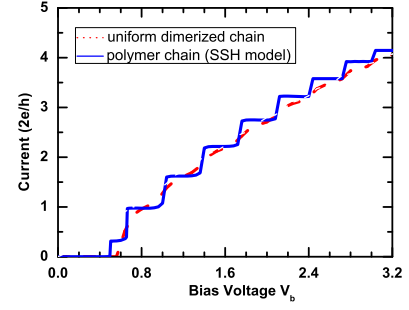


FIG. 5: Steady electronic current through a polymer chain of 30 sites (solid line). As a comparison, we also show the results for a uniform dimerized lattice (dashed line).

creases to 0.72 , the Fermi surface reaches the $n = \pm 2$ levels of the polymer and another pair of solitons is excited. When V_b increases again, soliton-lattice along with the corresponding soliton-lattice energy band is formed (Fig. 4(d) and Fig. 2(c)). From the results we presented here, we conclude that the electronic transport through a polymer chain is accomplished completely through the soliton-lattice energy band.

C. Nonequilibrium Electronic Current

In Fig. 5, we show the nonequilibrium electronic current through a chain with 30 sites. It's clear that when bias voltage V_b is below a critical value about 0.6 , the current I is zero, which indicates a gap about 0.6 width existing in the energy band under these bias voltages. And the step-like feature in current-voltage curve is a result of the finite size effect and can be explained by the gap shifted to match the Fermi levels of reservoirs, as shown in Fig. 3. As a comparison, we have also shown the current through a chain of a “uniform dimerized”, where the staggered lattice order parameter is taken to be independent of the site, *i.e.* $y_n = y$ for all sites n . It can be seen that the step-like feature disappears for a uniform dimerized lattice. The reason is clearly seen from the transmission rate $T(\epsilon)$ of a uniform dimerized chain, shown in Fig. 6, where a band gap reduction by increasing the bias voltage is clear seen while no band shift be seen.

D. Nonequilibrium Peierls Transition (NEPT)

In a one-dimensional system, the lattice is not stable against a $2k_F$ lattice distortion, which is known as the Peierls transition.¹⁶ For example, the ground state of a half-filled electronic system, such as polyacetylene, should be with a dimerized lattice at the temperature below a critical temperature. Ajisaka, *et al.*,¹⁴ considered a sandwich structure that is an open chain coupled with two metal electrodes, in which the chain is treated

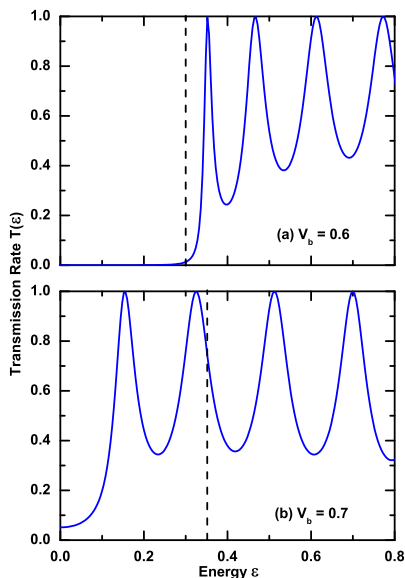


FIG. 6: The transmission rate $T(\epsilon)$ through a uniform dimerized chain of 30 sites for the bias voltage $V_b = 0.6$ (a) and 0.7 (b).

by the Takayama-Lin-Liu-Maki (TLM) model,¹⁷ a continuum version of the SSH model while the metal electrodes are described by reservoirs of free electrons. For a “uniform dimerized” lattice, they showed analytically that when the whole system is standing in nonequilibrium steady states, a NEPT between ordered and normal phases is found induced by the bias voltage V_b . The lattice is dimerized at the bias voltage below a critical value; otherwise the lattice will be uniform, *i.e.* $y = 0$.

Our analytical derivation for a uniform dimerized SSH chain at thermodynamic limit is given in the appendix C. No different result is found between the continuum TLM model and the discrete SSH model for the NESS. And numerical results for a lattice with finite sites are shown in Fig. 7(a). A jump of the order parameter y occurs at bias voltage about 0.6, which is the critical value that electrons from the reservoirs can flow through the polymer chain. As a comparison, we also show the result at thermodynamic limit, which seems to us the jump as a sign of the NEPT.

In Fig. 7(b), we show results for a lattice allowed to relax. Here we introduce a parameter \bar{y} , that is defined as

$$\bar{y}^2 = \frac{1}{N-1} \sum_{n=1}^{N-1} y_n^2, \quad (24)$$

to represent the degree of lattice distortion. It is clear from the figure that \bar{y} could reduce to 0.03 at least, not zero, which is different from that for a uniform dimerized chain. At the same time, we still see a jump at the bias voltage 0.6. These are contradict signs for the NEPT.

To clarify the NEPT for a chain with soliton excitation, we give the order parameter \bar{y} , in Fig. 7(c), for an

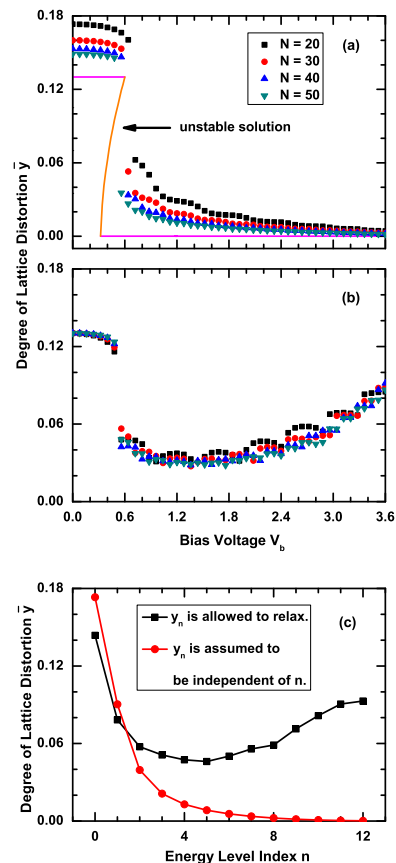


FIG. 7: Degree of lattice distortion \bar{y} of a polymer chain with 20, 30, 40 and 50 sites under different bias voltages V_b and (a) the lattice is restricted to be uniform and (b) is allowed to relax. (c) Degree of lattice distortion of an isolated polymer chain (30 sites) with different occupation n , which indicates the levels between $-n$ and $+n$ being singly occupied, as is shown in Fig. 4. In (a), \bar{y} of a polymer chain at thermodynamic limit is shown. Stable solution is represented by magenta line while unstable by orange line.

isolated polymer chain with different occupation n , which indicates the levels between $-n$ and $+n$ being singly occupied, as is shown in Fig. 4. The consistent with the results shown in Fig. 7 (a) and (b) told us that the lattice configure at nonequilibrium steady state with a bias voltage should be in correspondence with that an isolated chain with electronic excitations. With this, we can conclude that the NEPT does not survive the lattice relaxation and the soliton excitations, since the electronic excitations in an isolated chain only cause soliton excitations and the formation of a soliton lattice.¹⁵

IV. CONCLUSIONS

We have studied the steady current and the lattice configuration in a metal/polymer/metal structure with the metal electrodes treated as infinite reservoirs and the polymer chain described by the discrete SSH model of

electron-lattice interactions. Since the reservoirs are infinite, the whole system can reach a nonrilibrium steady state (NESS) with persistent particle flow. In this situation, it is the scattering states to be complete eigenstates of the whole system and the scattering state operators satisfy the Fermi distribution. Using the scattering state operator method, we show that in NESS, the solitons could be excited. Nonequilibrium Peierls transition does not survive the soliton excitations and the soliton-lattice is formed at thermodynamic limit. And it is the soliton-lattice energy band, not the conduction or the valence band, that provides the channels for electronic transport.

V. ACKNOWLEDGMENTS

The authors acknowledge the financial supports from the National Natural Science Foundation of China and the National Basic Research Program of China (Grant No. 2012CB921402 and 2009CB929204).

Appendix A: Calculation of the functions $F_n^{(a)}(\epsilon)$

Based on Eq.(10), (11), and (13), we denote

$$\frac{F_{n+1}^{(L)}(\epsilon)}{F_n^{(L)}(\epsilon)} = -\frac{\Sigma_n^{(L)}(\epsilon)}{t_n}, \quad \frac{F_n^{(R)}(\epsilon)}{F_{n+1}^{(R)}(\epsilon)} = -\frac{\Sigma_{n+1}^{(R)}(\epsilon)}{t_n} \quad (\text{A1})$$

for $n = 1, 2, \dots, N-1$, then the self-energies $\Sigma_n^{(L)}(\epsilon)$ and $\Sigma_n^{(R)}(\epsilon)$ satisfy following iteration relations

$$\Sigma_n^{(L)}(\epsilon) = \frac{t_n^2}{\epsilon - \Sigma_{n+1}^{(L)}(\epsilon)}, \quad \Sigma_{n+1}^{(R)}(\epsilon) = \frac{t_n^2}{\epsilon - \Sigma_n^{(R)}(\epsilon)}, \quad (\text{A2})$$

with

$$\Sigma_N^{(L)}(\epsilon) = -i\Gamma_R, \quad \Sigma_1^{(R)}(\epsilon) = -i\Gamma_L. \quad (\text{A3})$$

Now we obtain

$$F_n^{(a)}(\epsilon) = \frac{c_n^{(a)}(\epsilon)}{\epsilon - \Sigma_n^{(L)}(\epsilon) - \Sigma_n^{(R)}(\epsilon)}, \quad (\text{A4})$$

where

$$c_n^{(L)}(\epsilon) = \prod_{m=1}^{n-1} \left(-\frac{\Sigma_{m+1}^{(R)}(\epsilon)}{t_m} \right) \quad (\text{A5})$$

for $n \geq 2$ and $c_1^{(L)}(\epsilon) = 1$, and

$$c_n^{(R)}(\epsilon) = \prod_{m=n}^{N-1} \left(-\frac{\Sigma_m^{(L)}(\epsilon)}{t_m} \right) \quad (\text{A6})$$

for $n \leq N-1$ and $c_N^{(R)}(\epsilon) = 1$.

Appendix B: Calculation of the current flow

The current flow from the left reservoir to the polymer chain is given as

$$I_L = -\frac{2e}{\hbar} \sum_{k\sigma} g_{Lk} \text{Im} \langle d_{Lk\sigma}^\dagger c_{1,\sigma} \rangle, \quad (\text{B1})$$

and similarly, the current from the site n of the chain to the site $n+1$ is,

$$I_n = \frac{2e}{\hbar} t_n \sum_{\sigma} \text{Im} \langle c_{n,\sigma}^\dagger c_{n+1,\sigma} \rangle. \quad (\text{B2})$$

Based on the Eq.(10), (13), and (15), we have

$$\begin{aligned} \langle d_{Lk\sigma}^\dagger c_{1,\sigma} \rangle &= g_{Lk} F_1^{(L)}(\epsilon_{Lk}) f_L(\epsilon_{Lk}) + \sum_{ak'} g_{ak'}^2 |F_1^{(a)}(\epsilon_{ak'})|^2 \frac{g_{Lk}}{\epsilon_{ak'} - \epsilon_{Lk} - i\eta} f_a(\epsilon_{ak'}) \\ &= g_{Lk} \left[F_1^{(L)}(\epsilon_{Lk}) f_L(\epsilon_{Lk}) + i\Gamma_L |F_1^{(L)}(\epsilon_{Lk})|^2 f_L(\epsilon_{Lk}) + i\Gamma_R |F_1^{(R)}(\epsilon_{Lk})|^2 f_R(\epsilon_{Lk}) \right], \end{aligned} \quad (\text{B3})$$

where we have used the definition of DOS of the reservoirs (12) in the large bandwidth limit. Then we have

$$I_L = \frac{4e}{\hbar} \frac{\Gamma_L}{\pi} \int d\epsilon \left\{ -\text{Im} \{ F_1^{(L)}(\epsilon) \} f_L(\epsilon) - \Gamma_L |F_1^{(L)}(\epsilon)|^2 f_L(\epsilon) - \Gamma_R |F_1^{(R)}(\epsilon)|^2 f_R(\epsilon) \right\}, \quad (\text{B4})$$

where we have used $\sum_k g_{ak}^2 f(\epsilon_{ak}) = \int d\epsilon f(\epsilon) \sum_k g_{ak}^2 \delta(\epsilon - \epsilon_{ak}) = (\Gamma_a/\pi) \int d\epsilon f(\epsilon)$ for any function $f(\epsilon)$. Furthermore, we have $\text{Im} [F_1^{(L)}(\epsilon)] = -\Gamma_L |F_1^{(L)}(\epsilon)|^2 - t_1 \text{Im} [F_1^{(L)*}(\epsilon) F_2^{(L)}(\epsilon)]$ from Eq.(A1) and (A4), so that

$$I_L = \frac{2e}{\hbar} \frac{2\Gamma_L}{\pi} \int d\epsilon \left\{ t_1 \text{Im} [F_1^{(L)*}(\epsilon) F_2^{(L)}(\epsilon)] f_L(\epsilon) - \Gamma_R |F_1^{(R)}(\epsilon)|^2 f_R(\epsilon) \right\}. \quad (\text{B5})$$

Now we see that the above expression goes to Eq.(20) if we can show

$$t_1 \text{Im} \left[F_1^{(L)*}(\epsilon) F_2^{(L)}(\epsilon) \right] = \Gamma_R |F_1^{(R)}(\epsilon)|^2. \quad (\text{B6})$$

For that, from the Eq.(A1), we have

$$t_n \text{Im} \left[F_n^{(L)*}(\epsilon) F_{n+1}^{(L)}(\epsilon) \right] = -\text{Im} \Sigma_n^{(L)}(\epsilon) |F_n^{(L)}(\epsilon)|^2, \quad (\text{B7})$$

together with Eq.(A2), we have

$$\text{Im} \Sigma_n^{(L)}(\epsilon) |F_n^{(L)}(\epsilon)|^2 = \text{Im} \Sigma_{n-1}^{(L)}(\epsilon) |F_{n-1}^{(L)}(\epsilon)|^2, \quad (\text{B8})$$

then we get

$$t_n \text{Im} \left[F_n^{(L)*}(\epsilon) F_{n+1}^{(L)}(\epsilon) \right] = t_{n-1} \text{Im} \left[F_{n-1}^{(L)*}(\epsilon) F_n^{(L)}(\epsilon) \right], \quad (\text{B9})$$

which leads directly to

$$\begin{aligned} t_n \text{Im} \left[F_n^{(L)*}(\epsilon) F_{n+1}^{(L)}(\epsilon) \right] &= t_{N-1} \text{Im} \left[F_{N-1}^{(L)*}(\epsilon) F_N^{(L)}(\epsilon) \right] \\ &= \Gamma_R |F_N^{(L)}(\epsilon)|^2. \end{aligned} \quad (\text{B10})$$

The equality

$$F_N^{(L)}(\epsilon) = F_1^{(R)}(\epsilon) \quad (\text{B11})$$

is easy to be verified directly from the expressions of functions $F_n^{(a)}(\epsilon)$ obtained from Eq.(A4), which does not require the central inversion symmetry of the coupling with the reservoirs and the lattice configuration. Then we proved Eq.(B6).

Similarly, we have

$$\begin{aligned} \langle c_{n,\sigma}^\dagger c_{n+1,\sigma} \rangle &= \sum_{ak} |g_{ak}|^2 F_n^{(a)*}(\epsilon_{ak}) F_{n+1}^{(a)}(\epsilon_{ak}) f_a(\epsilon_{ak}) \\ &= \sum_a \frac{\Gamma_a}{\pi} \int d\epsilon F_n^{(a)*}(\epsilon) F_{n+1}^{(a)}(\epsilon) f_a(\epsilon), \end{aligned} \quad (\text{B12})$$

so that the current of the Eq.(B2) becomes

$$I_n = \frac{2e}{\hbar} \frac{2}{\pi} \sum_a \Gamma_a \int d\epsilon t_n \text{Im} \left[F_n^{(a)*}(\epsilon) F_{n+1}^{(a)}(\epsilon) \right] f_a(\epsilon). \quad (\text{B13})$$

Doing the same as Eq.(B9), we have

$$\begin{aligned} t_n \text{Im} \left[F_n^{(R)*}(\epsilon) F_{n+1}^{(R)}(\epsilon) \right] &= t_1 \text{Im} \left[F_1^{(R)*}(\epsilon) F_2^{(R)}(\epsilon) \right] \\ &= -\Gamma_L |F_1^{(R)}(\epsilon)|^2, \end{aligned} \quad (\text{B14})$$

together with the Eq.(B10) and (B11), we show that I_n is independent of site index n , and finally $I_n = I_L = I$, which meets the requirement of a NESS.

Appendix C: The case of a uniform dimerized lattice at thermodynamic limit

From Appendix B, we rewrite the transmission rate in Eq.(21) as follows

$$T(\epsilon) = -4\Gamma_L |F_n^{(L)}(\epsilon)|^2 \text{Im} \Sigma_n^{(L)}(\epsilon). \quad (\text{C1})$$

From Eq.(A4) together with Eq.(A1) and (A2), we have

$$|F_n^{(L)}(\epsilon)|^2 = -\frac{1}{\Gamma_L} \frac{\text{Im} \Sigma_n^{(R)}(\epsilon)}{|\epsilon - \Sigma_n^{(L)}(\epsilon) - \Sigma_n^{(R)}(\epsilon)|^2}, \quad (\text{C2})$$

then we have

$$T(\epsilon) = \frac{4\text{Im} \Sigma_n^{(L)}(\epsilon) \text{Im} \Sigma_n^{(R)}(\epsilon)}{|\epsilon - \Sigma_n^{(L)}(\epsilon) - \Sigma_n^{(R)}(\epsilon)|^2}, \quad (\text{C3})$$

which has been shown to be a quantity independent of index n in the NESS.

The bond-charge density $\rho_{n,n+1}$ given in Eq.(23) can be written as

$$\rho_{n,n+1} = \sum_a \int d\epsilon p_n^{(a)}(\epsilon) f_a(\epsilon), \quad (\text{C4})$$

where

$$p_n^{(L)}(\epsilon) = \frac{4}{\pi t_n} \frac{\text{Re} \Sigma_n^{(L)}(\epsilon) \text{Im} \Sigma_n^{(R)}(\epsilon)}{|\epsilon - \Sigma_n^{(L)}(\epsilon) - \Sigma_n^{(R)}(\epsilon)|^2} \quad (\text{C5})$$

and

$$p_n^{(R)}(\epsilon) = \frac{4}{\pi t_n} \frac{\text{Re} \Sigma_{n+1}^{(R)}(\epsilon) \text{Im} \Sigma_{n+1}^{(L)}(\epsilon)}{|\epsilon - \Sigma_{n+1}^{(L)}(\epsilon) - \Sigma_{n+1}^{(R)}(\epsilon)|^2}. \quad (\text{C6})$$

For a polymer chain of a uniform dimerized lattice at the thermodynamic limit, $y_n = y$, the hopping constant $t_n = 1 + (-1)^n y$ (hereafter, $t_0 (= 1)$ as the unit of energies), and the self-energies $\Sigma_n^{(L)}(\epsilon)$ for site n being far away from both of the ends should satisfy the following self-consistent equations

$$\Sigma_n^{(L)}(\epsilon) = \frac{t_n^2}{\epsilon - \Sigma_{n+1}^{(L)}(\epsilon)}, \quad \Sigma_{n+1}(\epsilon) = \frac{t_{n+1}^2}{\epsilon - \Sigma_n(\epsilon)}, \quad (\text{C7})$$

where we have used $\Sigma_n^{(L)} = \Sigma_{n+2}^{(L)}$. Then, we have $\text{Im} \Sigma_n(\epsilon) = 0$ for $|\epsilon| > 2$ or $|\epsilon| < 2|y|$, while for $2|y| \leq |\epsilon| \leq 2$,

$$\Sigma_n^{(L)}(\epsilon) = \frac{\epsilon^2 + (-1)^n 4y}{2\epsilon} - i \frac{\sqrt{(4 - \epsilon^2)(\epsilon^2 - 4y^2)}}{2|\epsilon|}. \quad (\text{C8})$$

Similarly, $\Sigma_n^{(R)}(\epsilon)$ is obtained to be that of $\Sigma_n^{(L)}(\epsilon)$ replaced y by $-y$. From the self-energies we obtain the transmission rate $T(\epsilon) = 0$ for $|\epsilon| > 2$ or $|\epsilon| < 2|y|$ and

$T(\epsilon) = 1$ for $2|y| < |\epsilon| < 2$. And $p_n^{(L)}(\epsilon) = p_n^{(R)}(\epsilon) = p_n(\epsilon)$ as given below

$$p_n(\epsilon) = -\frac{\epsilon}{|\epsilon|\pi t_n} \frac{\epsilon^2 + (-1)^n 4y}{\sqrt{(4 - \epsilon^2)(\epsilon^2 - 4y^2)}} \quad (\text{C9})$$

for $2|y| < |\epsilon| < 2$ and vanishes otherwise.

The lattice dimerization y is determined by $f(y) = 0$ with the function $f(y)$ is given as

$$f(y) = \frac{2y}{\pi\lambda} - \frac{1}{N} \sum_n (-1)^n \rho_{n,n+1}, \quad (\text{C10})$$

where we have used the Hellmann-Feynman theorem. In the thermodynamic limit, the contribution of the sites close to the two ends, where the bond-charge density might be affected by the reservoirs, is negligible. Then we have

$$f(y) = \frac{2y}{\pi\lambda} - \frac{1}{2}(\rho_{2n,2n+1} - \rho_{2n+1,2n+2}) \quad (\text{C11})$$

with $2n$ being the site far away from the two ends so that the right hand of the above equation will be independent of index n . It's clear that the lattice dimerization y will

be independent of the couplings with reservoirs since the dominant bonds in thermodynamic limit are those far away from the two ends.

For a symmetric applied bias voltage $\mu_L = -\mu_R = V_b/2$ with $2 \geq V_b/2 \geq 2|y|$, the self-consistent equation for y becomes

$$y = \frac{\lambda y}{1 - y^2} \int_{-2}^{-V_b/2} d\epsilon \sqrt{\frac{4 - \epsilon^2}{\epsilon^2 - 4y^2}}. \quad (\text{C12})$$

The integration from $-V_b/2$ to $V_b/2$ in the above equation for $f_L(\epsilon)$ has been cancelled out due to the anti-symmetry of the integrand. For the bias voltage $V_b \leq 4|y|$, the integration in Eq.(C12) will be up to $-2|y|$ and the self-consistent equation for y will return back to the one for an isolated chain, independent of applied bias voltage V_b .

The lattice order parameter y under different bias voltage V_b can be obtained from Eq.(C12), shown in Fig. 7(a), from which a NEPT can be seen as that of the TLM model obtained by Ajisaka, *et al.*¹⁴ No different is found between the continuum TLM model and the discrete SSH model for the NESS.

* Email: cqw@fudan.edu.cn

¹ L. Lafferentz, F. Ample, H. Yu, S. Hecht, C. Joachim, and L. Grill, *Science* **323**, 1193 (2009).

² N. J. Tao, *Nature Nanotechnology* **1**, 173 (2006).

³ A. Nitzan and M. A. Ratner, *Science* **300**, 1384 (2003).

⁴ R. H. M. Smit, Y. Noat, C. Untiedt, N. D. Lang, M. C. van Hemert, and J. M. van Ruitenbeek, *Nature* **419**, 906 (2002).

⁵ M. A. Reed, C. Zhou, C. J. Muller, T. P. Burgin, and J. M. Tour, *Science* **278**, 252 (1997).

⁶ C. Joachim, J. K. Gimzewski, R. R. Schlittler, and C. Chavy, *Phys. Rev. Lett.* **74**, 2102 (1995).

⁷ C. Q. Wu, Y. Qiu, Z. An, and K. Nasu, *Phys. Rev. B* **68**, 125416 (2003).

⁸ A. Johansson and S. Stafström, *Phys. Rev. Lett.* **86**, 3602 (2001).

⁹ S. V. Rakhmanova and E. M. Conwell, *Appl. Phys. Lett.* **75**, 1518 (1999).

¹⁰ H. Haug and A.-P. Jauho, *Quantum Kinetics in Transport and Optics of Semiconductors*, Springer-Verlag (Berlin, 2008).

¹¹ S. Hershfield, *Phys. Rev. Lett.* **70**, 2134 (1993).

¹² J. E. Han, *Phys. Rev. B* **73**, 125319 (2006); *Phys. Rev. B* **75**, 125122 (2007); *Phys. Rev. Lett.* **99**, 236808 (2007); *Phys. Rev. B* **81**, 113106 (2010); *Phys. Rev. B* **81**, 245107 (2010).

¹³ W. P. Su, J. Schrieffer, and A. Heeger, *Phys. Rev. Lett.* **42**, 1698 (1979); *Phys. Rev. B* **22**, 2099 (1980).

¹⁴ S. Ajisaka, H. Nishimura, S. Tasaki, and I. Terasaki, *Prog. Theor. Phys.* **121**, 1289 (2009).

¹⁵ B. Horovitz, *Phys. Rev. Lett.* **46**, 742 (1981).

¹⁶ R. E. Peierls, *Quantum Theory of Solids*, Oxford University Press (London, 1955).

¹⁷ H. Takayama, Y. R. Lin-Liu, and K. Maki, *Phys. Rev. B* **21**, 2388 (1980).

